# Normal Human Brain Growth

Mallory R. Peterson[1,2,5], Venkateswararao Cherukuri[1,4], Joseph N. Paulson[6], Paddy Ssentongo[2], Abhaya V. Kulkarni[7,8], Benjamin C. Warf[9,10], Vishal Monga[4], Steven J. Schiff[1-3*]

[1]Center for Neural Engineering, Departments of [2]Engineering Science and Mechanics, [3]Neurosurgery, and Physics, and [4]School of Computer Science & Electrical Engineering, The Pennsylvania State University, University Park, Pennsylvania, USA. [5]Medical Scientist Training Program, The Pennsylvania State University College of Medicine, Hershey, Pennsylvania, USA. [6] Department of Biostatistics, Product Development, Genentech Inc., South San Francisco, San Francisco, CA, USA. [7]University of Toronto. [8]The Hospital for Sick Children.[9]Harvard Medical School.[10] Boston Children's Hospital. *email: steven.j.schiff@gmail.com

May 19, 2020

Abstract

Brain growth is affected by a broad range of childhood conditions that affect cognitive development, but definitive growth curves for the brain throughout childhood have not been available. We studied the brain volume growth from 1,067 normal MRI scans from 505 normal healthy children from birth through age 18. Brain volume peaked at 10-12 years of age. Males exhibited larger age-adjusted total brain volumes than females, and body size normalization procedures did not eliminate this difference. Other significant gender-based differences were found in cerebrospinal fluid (CSF) accumulation, grey and white matter volumes, and lateralization between left and right temporal lobes and hippocampi. A significant correlation between cognitive scores with brain volume was found in the years leading up to the adolescent brain volume peak. The ratio of brain to CSF volume, however, uncovered a universal age-dependent relationship independent of gender or body size. These findings enable the use of normative growth curves in managing a broad range of childhood disease where cognitive development and brain growth is impaired.

The study of brain size and growth has a long and contentious history(*1-4*). In the pre-MRI era, post-mortem studies provided insight into brain volume changes over the lifespan, but such methods suffered from inherent inaccuracies(*5*). The magnetic resonance imaging (MRI) era enabled detailed in-vivo volumetrics including components of the brain, but there has not been a definitive analysis of normal brain growth throughout the entire pediatric age range(*6-9*). We sought to create normative growth curves for the human brain in order to enable improved management of a broad range of childhood diseases where cognitive development and brain growth are impaired.

The MRI era has facilitated computational in vivo structural brain quantification, which we leveraged to analyze 1,067 MRI scans from healthy pediatric participants in the NIH Pediatric MRI Repository (https://nda.nih.gov), under an institutional data use agreement between The Pennsylvania State University and the National Institute of Mental Health. This MRI repository was developed based on a scaled-down United States (US) census with rigorous exclusion criteria, with the goal of providing a standard representation of the socioeconomic, gender, and ethnic distribution of healthy normal US children(*10*). The cross-sequential cohort contains participants in each year of life ranging from 13-days to 22-years old (Supplemental Figure 1).

Studies defining brain volume growth patterns in the MRI era have suffered from small sample sizes, limited algorithm technology, incomplete coverage of the pediatric age range, retrospective cohorts taken from clinical patients, and an inconsistent array of curve fitting techniques(*6-8, 11, 12*). The current study addresses these limitations to develop normative growth curves for the US pediatric population. This cross-sequential data includes 505 subjects

(259 female), of which the majority have two or three longitudinal MRI scan sets, leading to a total number of 1067 healthy MRI scans (Supplemental Figure 1c).

The T2 MRI images of the neonatal population were processed using the Developing Human Connectome Project (dHCP) Pipeline in order to appropriately segment the rapidly growing and incompletely myelinated brains(*13*). The T1 images of the older subjects were processed using the Computational Anatomy Toolbox (CAT) within the Statistical Parametric Mapping (SPM12) software(*14*). The resulting segmentation images (Supplemental Figure 2) were manually inspected to ensure appropriate labelling of these compartments and regions.

The volumes quantified by the dHCP and CAT12 pipelines were then fit using Smoothing Splines ANOVA (SSANOVA) with random effects (to account for the cross-sequential design of the study) to define time periods of significant differences between genders and hemispheres (Figure 1, 2 , and Supplemental Figure 3)(*15*). The volumes were also fit using Generalized Additive Models for Location, Scale, and Shape (GAMLSS) with a Box-Cox power exponential (BCPE) distribution (Supplemental Figures 4 and 5), which is the platform and distribution leveraged by the World Health Organization to develop their standard growth curves for weight, height, and head circumference(*16, 17*).

Males exhibited larger overall brain volumes than females throughout childhood (Figure 1a). The volume for females peaked at 10.7 years, and the volume for males peaked at 11.2 years, followed by a slow, but consistent decrease. Although this early adolescent peak has been noted(*11*), data from early childhood (< 4 years of age) was not previously incorporated. Cerebrospinal fluid (CSF) increased throughout childhood, with male fluid accumulation significantly larger than female after the third year of life (Figure 1b). Grey matter (Figure 1c)

peaked at 7.5 years for males and 7.4 years for females, while white matter (Figure 1d) continued to progressively increase into early adulthood(*18*). The ratio of grey/white matter (Figure 1e) showed an initial increase, peaking before 2 years of age and followed by a progressive decrease thereafter. Female grey/white matter ratios were significantly larger than male ratios between ages 9 and 11 although the difference was small (Figure 1e).

We performed body size normalization to assess if gender differences in brain volume persisted. Normalizing the brain by body size is not a new concept; allometry, or differential growth, of the brain with respect to body size was discussed in depth by D'Arcy Wentworth Thompson in 1917 in *On Growth and Form(19)*. Gould, in *The Mismeasure of Man*, attempted and failed to eliminate gender differences through body size normalization procedures(*1*). Nevertheless, much of the volumetric brain study in the MRI era has not accounted for anthropomorphic normalization. Figures 1f and 1g show brain volume normalized by height-for-age and weight-for-height, respectively, which did not eliminate the gender-based differences in volume. Muscle mass content, greater in males, has been correlated with larger brain volumes although not with higher cognitive capability(*20*). However, the ratio of brain to CSF volume demonstrated no significant gender differences at any age, without applying anthropomorphic normalization (Figure 1h).

Figure 2a and 2b show that there was no lateralizing difference in size between right and left hemispheres for males and females, nor for cerebellum, frontal, parietal, or occipital lobes (Supplemental Figure 2). Figure 2c and 2d show that the left temporal lobe was significantly larger than the right for both males and females, which has been controversial(*21*). In addition, the hippocampi were significantly larger on the right than the left side for both

genders (Figure 2e and 2f). Age-adjusted hippocampal and temporal lobe volume assessment may be of value in diagnosing and treating medically refractive epilepsy in childhood(*21*).

Cognitive scores showed a small but significant correlation with brain volume in the four years leading up to the peak in volume (Figure 3). The Mental Development Index (MDI) scores for infants from birth to age three were not significantly predicted by brain volume (Figure 3b), but the Weschler Abbreviated Scale of Intelligence (WASI) scores for ages 6-18 years were significantly correlated with brain volume z-scores (Figure 3a), as described previously(*22*). Usinga sliding window across age we found that the correlation between cognitive score and brain volume was significant for raw brain volume, age-adjusted brain volume z-score, and weight-for-height normalized volumes in the years immediately preceding the brain volume peak (Figure 3c-3e). This correlation is not maintained when separating into smaller cohorts by gender (Supplemental Figure 6).

In 1987, Roche et al created head circumference growth curves from studying 888 healthy US children(*23*), and such normative head circumference curves from US(*24*) and World Health Organization(*16, 25*) cohorts are now in routine clinical practice as indirect metrics of brain growth. Figure 4 illustrates the analogous GAMLSS pediatric brain volume growth curves for males and females (Figure 4a and 4b), with early brain volume growth and CSF volume insets included, as well as the brain/CSF ratio (Figure 4c and 4d) for a more comprehensive presentation of childhood normative brain growth suitable for clinical settings. The apparent universal nature of the age-dependent brain/CSF ratio, regardless of gender or body size, suggests that the role of this ratio warrants clinical investigation(*26*).

Brain volume measurement became a field of study of biological determinism pioneered by Samuel Morton in the mid-1800s(*1, 27*). Morton filled over 1000 cranial vaults with mustard seed and lead shot to determine brain volume, which he then compared between races and genders. A century and a half later Gould used Morton as a case study in scientific bias[1]. Decades after the publishing of these analyses in *The Mismeasure of Man*, arguments over biases and flaws continue in the assessment of the volume of the normal human brain(*2-4*).

Our findings demonstrate that for a broad spectrum of human disease affecting neurocognitive development and brain growth – ranging from neonatal infection(*28*) to malnutrition(*29*) and hydrocephalus(*30*) – measuring brain growth with respect to normative values is now feasible. The small association observed for brain size within the normal range with cognitive performance within the normal range will likely be magnified in children with disease early in life that substantially impacts brain growth. A major challenge for children's medicine is now how to construct the frameworks needed to improve cognitive outcomes by optimizing brain growth based upon interventions(*31*). We anticipate that these findings will enable more personalized optimization of treatment and care for a broad range of debilitating childhood conditions.

**Acknowledgements**

We are grateful to T. Sauer and S. Sinnar for helpful discussion, and to Y. Wang and J. Chai for technical help in compiling data. This research was supported by the Penn State and National Science Foundation Center for Healthcare Organization Transformation (CHOT) collaboration,

US National Institutes of Health grants R01HD085853 (VC, AK, BCW, VM, SJS), and the NIH Director's Transformative Award R01AI145057 (MRP, JNP, SJS).

**Author Contributions**

Conception and design: SJS, MRP. Acquisition of data: MRP, VC. Analysis and interpretation of data: MRP, VC, VM, JNP, AK, BCW, SJS. Drafting the article: MRP, SJS. Critically revising the article: all authors. Reviewed and approved submitted version of manuscript: all authors.

**Competing Interests**

The authors declare no competing interests.

## Supplementary Materials

### Cohort Characteristics

The MRI scans used in this study were taken from the NIH Pediatric MRI Repository (https://nda.nih.gov) under an institutional data use agreement (214908) between The Pennsylvania State University and the National Institute of Mental Health approved on January 14, 2019, and a determination (STUDY00010883) by the Penn State Institutional Review Borad that this activity does not meet the definition of human subject research and does not require IRB review and approval. This repository was developing using a scaled down United States census (in order to appropriately represent the demographic characteristics of the entire US pediatric population) and included rigorous exclusion criteria to ensure healthy participants with normal brain development. The repository aimed to achieve two-year longitudinal follow-up scans for individual participants, and was able to accomplish this for 378 of the subjects, making this a cross-sequential study(*10*). The cross-sequential format is ideal for the development of growth curves(*7, 32*). The number of subjects in this study was 505 (259 female), with a total of 1067 MRI scans due to the longitudinal nature of the cohort. The minimum age was 13 days, and the maximum age was 22 years, but only scans from subjects up to 18-years-old were included to develop growth curves representative of the pediatric age range. Scans existed for participants in each year of life throughout the pediatric age range, as seen in Supplemental Figure 1.

### Segmentation Algorithms

Currently, no single algorithm exists that can reliably segment both young infants and older subjects(*33, 34*). This is particularly due to the myelination changes that do not resolve until

approximately two years of age(*35*). These myelination changes lead to difficulty in establishing intensity thresholds between grey matter, white matter, and CSF(*35*). In order to maximize thresholding intensities, neonatal segmentation techniques most commonly rely on T2 weighted MRI scans, rather than T1 weighted scans that are the predominant scan type used in older cohort segmentation algorithms. Due to these reasons, two different algorithms were used in this study. The neonates were assessed using the Developing Human Connectome Project (dHCP) pipeline, which required T2 images and was run through a virtual Docker container to access a Linux computer system(*13*). The older subjects were assessed using the Computational Anatomy Toolbox 12 (CAT12) within the Statistical Parametric Mapping (SPM) platform using Matlab 2019b, which relies on T1 images(*14*). Each of the resulting scan sets was manually curated to ensure that appropriate skull-stripping and segmentation was accomplished. Upon establishing the volumes determined by each segmentation procedure, the accompanying atlases were used to compile volumes for the desired regions from smaller sections of the brain(*36, 37*).

**Smoothing Splines ANOVA**

The compartment differences between males and females were explored within the R platform using non-parametric Smoothing Splines ANOVA models with a random effects component added to account for the cross-sequential aspect of the data(*15*). The model included age and gender or hemisphere as main factors, as well as an interaction term. Time periods with significant gender or hemispheric differences were defined as regions where there was no overlap between the Bayesian 95% confidence intervals calculated for the gender and

hemispheric factors. These regions of significant difference were highlighted on the plotted models, and the time period of significance was documented as well.

**Generalized Additive Models for Location, Scale, and Shape (GAMLSS)**

The smooth growth curves used to fit the volumes and other growth metrics included in this study were developed using the Generalized Additive Models for Location, Scale, and Shape software implemented in R(*17*). The Box-Cox power exponential (BCPE) distribution, which was chosen by the World Health Organization (WHO) for their standard growth curves, was used to model the volumes in this study(*38*). This distribution models the median for a nonparametric assessment, and appropriately accounts for kurtosis and skewness within the data. The growth curves were fitted using the default RS algorithm and were smoothed using fractional polynomials of the third order(*17*). A random effects component was added to the curve modeling procedure in order to account for the longitudinal aspect of the data. For the total brain tissue growth curves, we utilized data for subjects between 18-22 years of age to set the 18 year old volume intercepts, and the perinatal volume data from Huppi et al to set the volume intercepts at birth(*39*).

In order to determine the peaks of the brain tissue and grey matter curves, cftool within Matlab 2019b was used to fit differentiable rational polynomial functions (which were applied as the smoothing function in the GAMLSS curves)(*40*). The significant gender and hemispheric differences were found using the Mann-Whitney U-test within Matlab 2019b. A Bonferroni correction was applied so that significance was established with $p<0.000066$.

The weight for height and height for age normalizations were accomplished by fitting a GAMLSS curve to the weight for height and height for age data from the NIH repository for each

gender. Based on these fits, percentiles were calculated for each subject, and the 50th percentile was set at 1, with percentiles above and below ranging from 0.5 to 1.5. The corresponding brain volume for each subject was then divided by this percentile value to achieve normalized brain volumes.

**Cognitive Score Correlations**

Cognitive scoring was included in the NIH Pediatric MRI Repository study, with Wechsler Abbreviated Scale of Intelligence (WASI) Tests undertaken on participants ranging from 6 years of age to 18 years of age. The infants (from birth to 3 years of age) were assessed using the Bayley Scales of Infant Development, Second Edition (BSID-II) Mental Development Index (MDI). We fit a linear mixed effects model (with subject identification as the random effects component) to the appropriate cognitive score using the brain volume z-score values. While the linear fits showed positive slopes for each metric, only the WASI scores showed a significant fixed effect for the brain volume z-score. Plots of the windowed correlation with a subpopulation value of 120 subjects and an overlap value of 20 subjects were developed for raw brain volume, brain volume z-score, and weight-for-height normalized volume z-score.

**Limitations**

While the growth curves developed in this study provide a standard representation of the United States pediatric population, they can only act as a reference and not as a standard for other geographic regions. Other growth curves specific to particular regions should be developed using healthy cohorts derived from those regions in order to provide appropriately representative global standards.

**Data Availability**

The volumes used to create the SSANOVA and GAMLSS growth curves presented here are provided in a spread sheet supplied in the online supplemental material (Supplemental Extended Data).

**References**


1. S. J. Gould, *The mismeasure of man*. (First edition. New York : Norton, [1981] ©1981, 1981).
2. J. E. Lewis *et al.*, The mismeasure of science: Stephen Jay Gould versus Samuel George Morton on skulls and bias. *PLoS Biol* **9**, e1001071 (2011).
3. M. Weisberg, D. B. Paul, Morton, Gould, and Bias: A Comment on "The Mismeasure of Science". *PLoS Biol* **14**, e1002444 (2016).
4. Mismeasure for mismeasure. *Nature* **474**, 419-419 (2011).
5. A. S. Dekaban, Changes in brain weights during the span of human life: relation of brain weights to body heights and body weights. *Ann Neurol* **4**, 345-356 (1978).
6. A. Pfefferbaum *et al.*, A Quantitative Magnetc Resonance Imaging Study of Changes in Brain Morphology From Infancy to Late Adulthood. *JAMA Neurology* **51**, (1994).
7. E. Courchesne *et al.*, Normal brain development and aging: Quantitative analysis at in vivo MR imaging in healthy volunteers. *Radiology* **216**, 672-682 (2000).
8. M. Peterson, B. C. Warf, S. J. Schiff, Normative human brain volume growth. *Journal of Neurosurgery: Pediatrics* **21**, 478-485 (2018).
9. J. N. Giedd *et al.*, Brain development during childhood and adolescence: a longitudinal MRI study. *Nat Neurosci* **2**, 861-863 (1999).
10. A. C. Evans, The NIH MRI study of normal brain development. *NeuroImage* **30**, 184-202 (2006).
11. J. N. Giedd *et al.*, Quantitative magnetic resonance imaging of human brain development: ages 4-18. *Cereb Cortex* **6**, 551-560 (1996).
12. A. McAllister *et al.*, Quantitative Synthetic MRI in Children: Normative Intracranial Tissue Segmentation Values during Development. *AJNR. American journal of neuroradiology* **38**, 2364-2372 (2017).
13. A. Makropoulos *et al.*, The developing human connectome project: A minimal processing pipeline for neonatal cortical surface reconstruction. *Neuroimage* **173**, 88-112 (2018).
14. C. Gaser, R. Dahnke, CAT-a computational anatomy toolbox for the analysis of structural MRI data. *HBM* **2016**, 336-348 (2016).
15. C. Gu, *Smoothing Spline ANOVA Models*. (Springer, 2002).
16. E. Borghi *et al.*, Construction of the World Health Organization child growth standards: Selection of methods for attained growth curves. *Statistics in Medicine* **25**, 247-265 (2006).
17. R. A. Rigby, D. M. Stasinopoulos, P. W. Lane, Generalized additive models for location, scale and shape. *Journal of the Royal Statistical Society. Series C: Applied Statistics* **54**, 507-554 (2005).

18. K. Narvacan, S. Treit, R. Camicioli, W. Martin, C. Beaulieu, Evolution of deep gray matter volume across the human lifespan. *Human Brain Mapping* **38**, 3771-3790 (2017).
19. D. A. W. Thompson, *On Growth and Form*. (Cambridge University Press, Cambridge, 1917).
20. A. H. M. Kilgour, O. M. Todd, J. M. Starr, A systematic review of the evidence that brain structure is related to muscle structure and their relationship to brain and muscle function in humans over the lifecourse. *BMC Geriatr* **14**, 85-85 (2014).
21. J. G. Mandell *et al.*, Volumetric brain analysis in neurosurgery: Part 3. Volumetric CT analysis as a predictor of seizure outcome following temporal lobectomy. **15**, 133 (2015).
22. A. L. Reiss, M. T. Abrams, H. S. Singer, J. L. Ross, M. B. Denckla, Brain development, gender and IQ in children: A volumetric imaging study. *Brain* **119**, 1763-1774 (1996).
23. A. F. Roche, D. Mukherjee, S. Guo, W. M. Moore, Head Circumference Reference Data: Birth to 18 Years. *Pediatrics* **79**, 706-712 (1987).
24. C. O. RJ Kuczmarski, LM Grummer-Strawn, *CDC Growth Charts: United States*. Advance data from vital and health statistics (National Center for Health Statistics, Hyattsville, MD, 2000), vol. 314.
25. D. C. M de Onis, C Garza, AW Onyango, WHO Child Growth Standards. *Acta Paediatrica*, (2006).
26. M. K. Rasmussen, H. Mestre, M. Nedergaard, The glymphatic pathway in neurological disorders. *Lancet Neurol* **17**, 1016-1024 (2018).
27. S. G. Morton, *Crania americana*
*A comparative view of the skulls of various aboriginal nations of North and South America*. (Philadelphia, 1839).
28. A. Grinberg *et al.*, Volumetric MRI Study of the Brain in Fetuses with Intrauterine Cytomegalovirus Infection and Its Correlation to Neurodevelopmental Outcome. *American Journal of Neuroradiology* **40**, 353-358 (2019).
29. K. Tiwari *et al.*, Impact of malnutrition on head size and development quotient. *International Journal of Research in Medical Sciences* **5**, 4 (2017).
30. A. V. Kulkarni *et al.*, Endoscopic Treatment versus Shunting for Infant Hydrocephalus in Uganda. *New England Journal of Medicine* **377**, 2456-2464 (2017).
31. J. W. S. Lenhart, *Optimal Control Applied to Biological Models*. ( Chapman and Hall/CRC, New York, 2007).
32. P. J. Diggle, P. Heagerty, K.-Y. Liang, S. L. Zeger, Analysis of Longitudinal Data. 379-379 (2002).
33. C. N. Devi, A. Chandrasekharan, V. K. Sundararaman, Z. C. Alex, Neonatal brain MRI segmentation: A review. *Computers in Biology and Medicine* **64**, 163-178 (2015).
34. Y. Ding *et al.*, Using Deep Convolutional Neural Networks for Neonatal Brain Image Segmentation. *Frontiers in Neuroscience* **14**, (2020).
35. A. Makropoulos, S. J. Counsell, D. Rueckert, A review on automatic fetal and neonatal brain MRI segmentation. *NeuroImage* **170**, 231-248 (2018).
36. A. Hammers *et al.*, Three-dimensional maximum probability atlas of the human brain, with particular reference to the temporal lobe. *Human Brain Mapping* **19**, 224-247 (2003).

37. I. S. Gousias *et al.*, Automatic segmentation of brain MRIs of 2-year-olds into 83 regions of interest. *NeuroImage* **40**, 672-684 (2008).
38. R. A. Rigby, D. M. Stasinopoulos, Smooth centile curves for skew and kurtotic data modelled using the Box-Cox power exponential distribution. *Stat Med* **23**, 3053-3076 (2004).
39. P. S. Huppi *et al.*, Quantitative magnetic resonance imaging of brain development in premature and mature newborns. *Ann Neurol* **43**, 224-235 (1998).
40. *Curve fitting toolbox : for use with MATLAB® : user's guide*. (Version 1. Natick, MA : MathWorks, 2001., 2001).

**Figure Legends**

**Figure 1**. Brain Compartment Gender Differences. SSANOVA models with random effects were fit to **a)** total brain volume (cc), **b)** cerebrospinal fluid (CSF) (cc), **c)** grey matter (cc), **d )**white matter (cc), **e)** grey to white matter ratio, **f)** height for age normalized brain volume, **g)** weight for height normalized brain volume, and **h)** brain to CSF ratio. For each plot, the male data is shown in blue and the female data in red. The dashed line represents the fit, with the two solid lines on either side showing the Bayesian 95% confidence intervals. The upper and lower intervals for the right and left sides overlap throughout the entire time frame for the brain/CSF ratio, and therefore there are no statistically significant differences at any age. For the other plots, time periods of significant differences where the intervals do not overlap are shown in yellow.

**Figure 2**. Brain Region Hemispheric Differences. SSANOVA models with random effects were fit to **a,b)** hemispheres (cc), **c,d)** temporal lobes (cc), and **e,f)** hippocampi (cc). Female regional growth curves from birth to 18-years-old are shown in the left column, and the corresponding male regional curves are shown in the right column. For each plot, the left side is shown in green and the right side in purple. The dashed line represents the fit, with the two solid lines

on either side showing the Bayesian 95% confidence intervals. The upper and lower intervals for the right and left sides overlap throughout the entire time frame for the hemispheres, and therefore there are no statistically significant differences. For the temporal lobes and hemispheres, time periods of significant differences where the intervals do not overlap are shown in yellow.

**Figure 3.** Cognitive Score Correlations. Two cognitive scores were used, the Mental Development Index (MDI) for infants from birth to age 3, and the Wechsler Abbreviated Scale of Intelligence (WASI) Tests for adolescents aged 6 to 18. Linear mixed effects models were fit for **a)** the relationship between MDI and brain volume z-score, as well as **b)** the relationship between WASI and brain volume z-score. Correlation association plots were developed with a subpopulation of 120 and overlap of 20 subjects to show the Pearson Correlation between cognitive score and **c)** raw brain volume, **d)** brain volume z-score, and **e)** weight-for-height normalized brain volume z-score as a function of age.

**Figure 4**. Standard Brain Volume Growth Curves. To provide a standard tool for researchers and clinicians, normal curves resembling head circumference growth curves were fit using GAMLSS to show the 3$^{rd}$, 15$^{th}$, 50$^{th}$, 85$^{th}$, and 97$^{th}$ percentiles of normal brain volume growth for **a)** females and **b)** males, as well as the ratio of brain to CSF for **c)** females and **d)** males. The growth curves were modeled using a Box-Cox power exponential distribution and smoothed using fractional polynomials. Both male and female brain volume plots include insets for brain growth from birth to age 2, as well as CSF accumulation from birth to age 18, in order to provide a comprehensive picture of brain growth dynamics in the pediatric age range.

**Supplemental**

**Supplemental Figure 1**. Cohort Characteristics. Data from each age group from 13 days to 22 years was included in the cohort, for both **a)** males and **b)** females. The cross-sequential study included **c)** 505 total subjects, with most subjects having between 2 and 3 longitudinal visits (separated by 2 years). For this study, only scans from 13 days to 18 years were included in order to focus on the pediatric age range.

**Supplemental Figure 2.** Segmentation Results. Two different algorithms for volume quantification were used, one for the neonates and one for the older cohort. As an example, a **a)** T2 MRI scan from a 16-day-old female is shown. This scan was processed through the dHCP pipeline to produce a **c)** segmentation including grey matter, CSF, and white matter. On the right, the **b)** T1 MRI scan from an older patient (a 15-year-old male) is shown. This scan was processed using the CAT12 pipeline within SPM to produce the **d)** segmentation including grey matter, CSF, and white matter.

**Supplemental Figure 3.** Brain Lobe and Cerebellum Hemispheric Differences. SSANOVA models with random effects were fit to **(a,b)** frontal lobes (cc), **(c,d)** parietal lobes (cc), **(e,f)** occipital lobes (cc), **(g,h)** and cerebella (cc). Female regional growth curves from birth to 18-years-old are shown in the left column, and the corresponding male regional curves are shown in the right column. For each plot, the left side is shown in green and the right side in purple. The dashed line represents the fit, with the two solid lines on either side showing the Bayesian 95% confidence intervals. The upper and lower intervals for the right and left sides overlap throughout the entire time frame for each region, and therefore there are no statistically significant differences.

**Supplemental Figure 4.** Brain Compartment Standard Growth Curves. Growth curves from birth to 18-years-old developed with Generalized Additive Models for Location, Shape, and Scale are shown for males in blue and females in red, with the solid median accompanied by dotted one and two standard deviations above and below. Each growth curve was modeled using a Box-Cox power exponential distribution and smoothed using fractional polynomials. The yellow boxes represent Bonferroni corrected significant differences ($p<0.00006$) between males and females for each year, obtained using the Mann-Whitney test. This univariate testing was applied to obtain conservative estimates of the differences in the data for each year of life. The standard curves plotted include **a)** total brain volume (cc), **b)** CSF, **c)** grey matter, **d )**white matter, **e)** the ratio of total brain volume to CSF, **f)** the ratio of grey to white matter, **g)** head circumference (cm), **h)** height normalized brain volume, **i )** weight for height normalized brain volume, and **j)** height for age normalized brain volume.

**Supplemental Figure 5.** Brain Region Standard Growth Curves. Female regional growth curves from birth to 18-years-old are shown in the left column, and the corresponding male regional curves are shown in the right column, all developed using Generalized Additive Models for Location, Shape, and Scale. Each growth curve was modeled using a Box-Cox power exponential distribution and smoothed using fractional polynomials. Left regions are shown in green, and right regions are shown in purple, with the solid median accompanied by dotted one and two standard deviations above and below. The yellow boxes represent Bonferroni corrected significant differences ($p<0.00006$) between left and right compartments in that year, obtained using the Mann-Whitney test. The green boxes represent significant differences between the left region for males and females in that year, while the purple boxes represent

significant differences between the right region for males and females in that year. The standard curves plotted include **(a,b)** hemispheres (cc), **(c,d)** frontal lobes (cc), **(e,f)** temporal lobes (cc), **(g,h)** parietal lobes (cc),**(i,j)** occipital lobes (cc), **(k,l)** cerebella (cc), and **(m,n)** hippocampi (cc).

**Supplemental Figure 6.** Gender Cognitive Score Correlations. Plots were developed with a subpopulation of 120 and overlap of 20 subjects to show the Pearson Correlation and confidence intervals between cognitive score and **(a,b)** raw brain volume, **(c,d)** brain volume z-score, and **(e,f)** weight-for-height normalized brain volume z-score at different ages for both females and males.

**Expanded Data:**

Supplemental Excel File: Supplemental_Master_File.xlsm

Figure 1

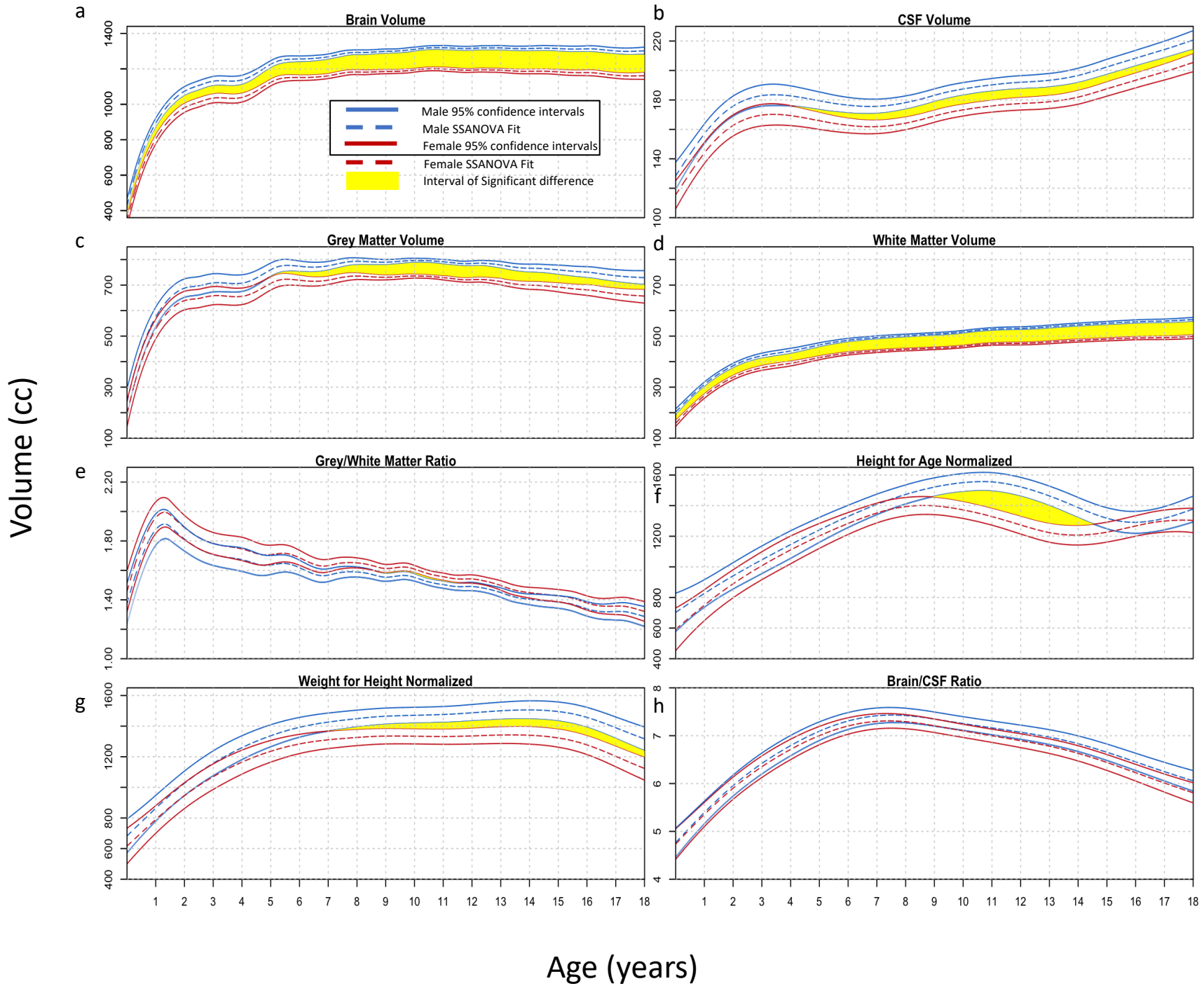
a
Brain Volume
b
CSF Volume
c
Grey Matter Volume
d
White Matter Volume
e
Grey/White Matter Ratio
f
Height for Age Normalized
g
Weight for Height Normalized
h
Brain/CSF Ratio
Male 95% confidence intervals
Male SSANOVA Fit
Female 95% confidence intervals
Female SSANOVA Fit
Interval of Significant difference
Volume (cc)
Age (years)

Figure 2

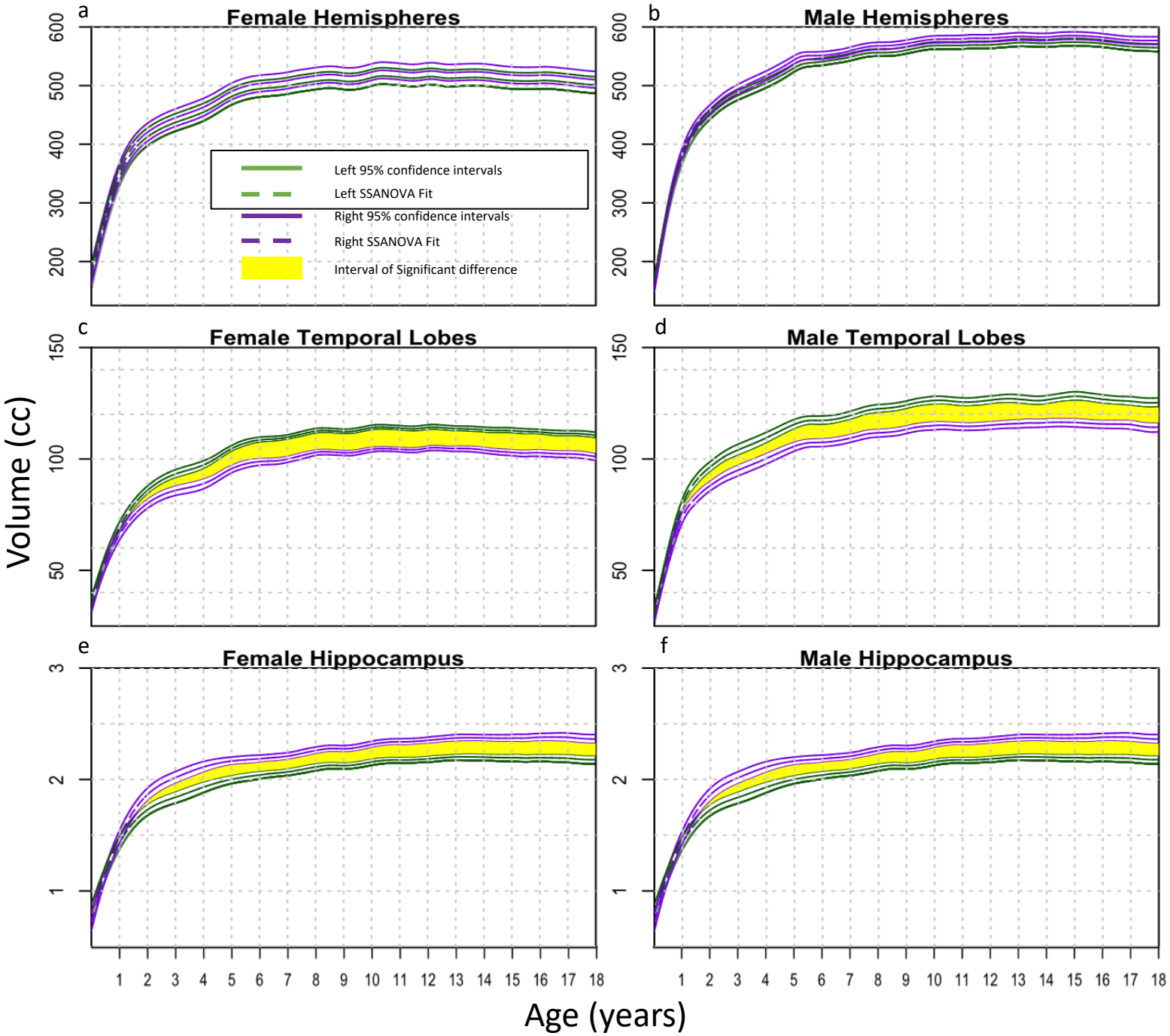
a
Female Hemispheres
b
Male Hemispheres
c
Female Temporal Lobes
d
Male Temporal Lobes
e
Female Hippocampus
f
Male Hippocampus
Left 95% confidence intervals
Left SSANOVA Fit
Right 95% confidence intervals
Right SSANOVA Fit
Interval of Significant difference
Volume (cc)
Age (years)

Figure 3

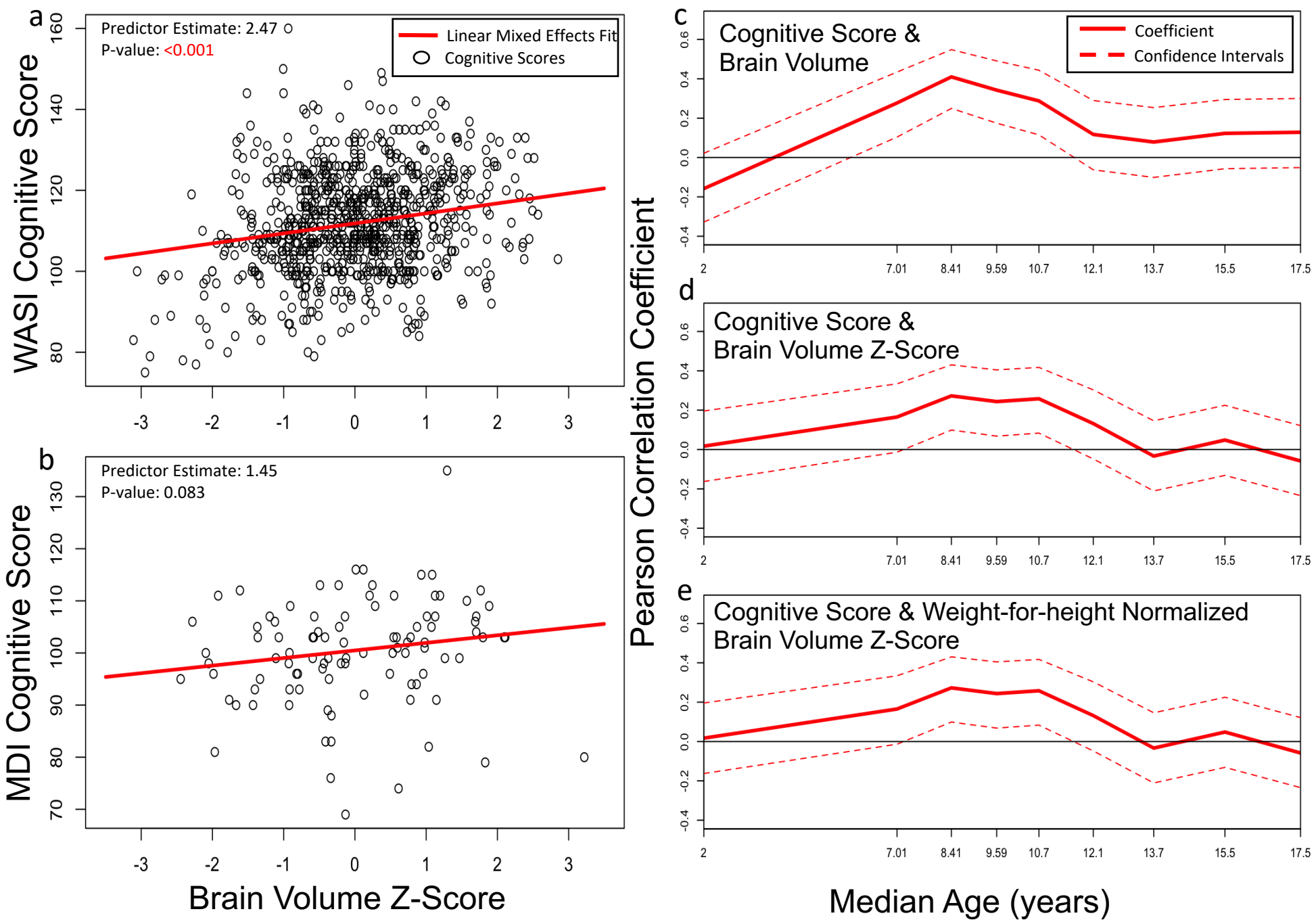
a
Predictor Estimate: 2.47
P-value: <0.001
Linear Mixed Effects Fit
Cognitive Scores
WASI Cognitive Score
b
Predictor Estimate: 1.45
P-value: 0.083
MDI Cognitive Score
Brain Volume Z-Score
c
Cognitive Score &
Brain Volume
Coefficient
Confidence Intervals
d
Cognitive Score &
Brain Volume Z-Score
e
Cognitive Score & Weight-for-height Normalized
Brain Volume Z-Score
Pearson Correlation Coefficient
Median Age (years)

Figure 4

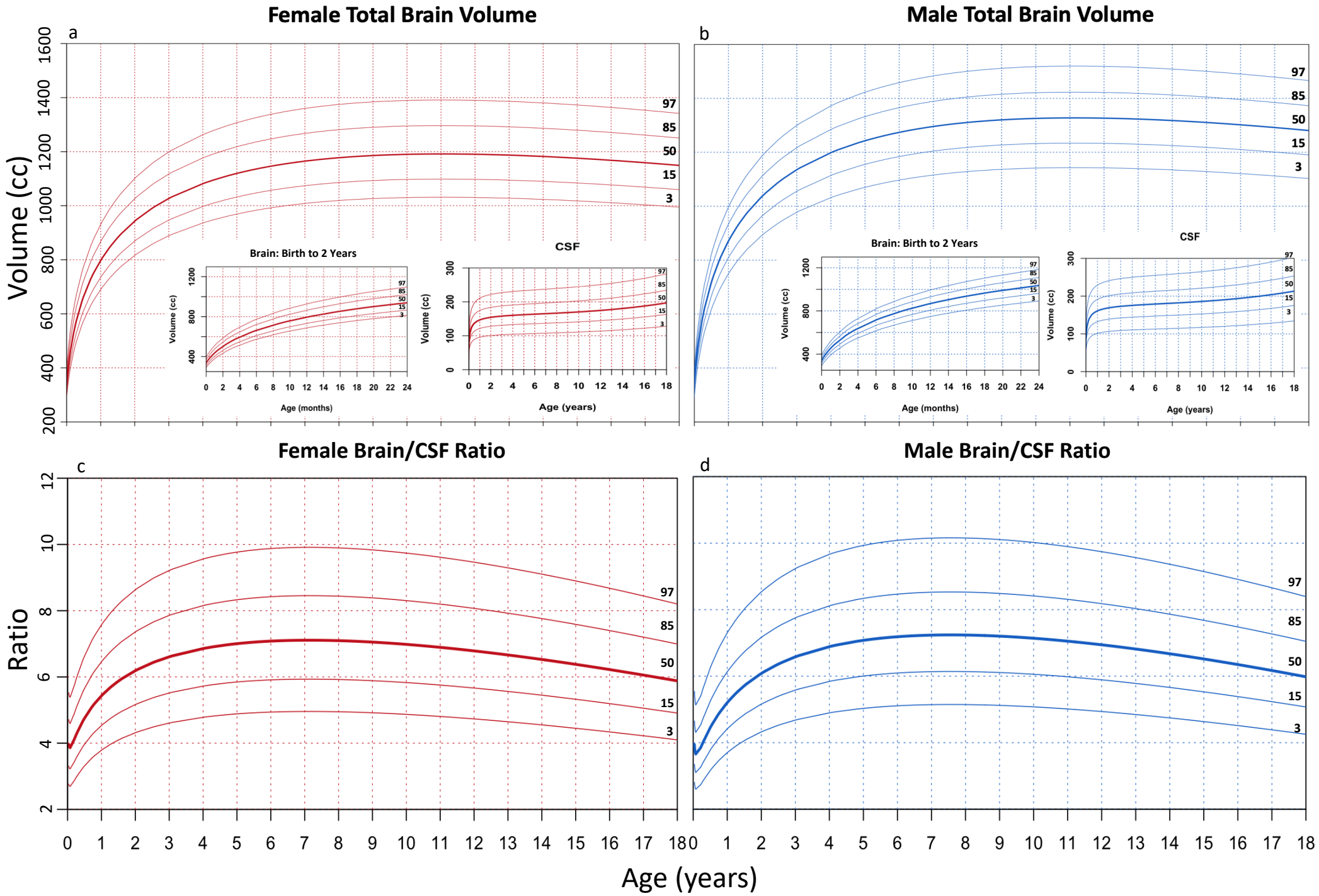
Female Total Brain Volume
a
Volume (cc)
97
85
50
15
3
Brain: Birth to 2 Years
Volume (cc)
Age (months)
CSF
Volume (cc)
Age (years)
Male Total Brain Volume
b
Brain: Birth to 2 Years
Volume (cc)
Age (months)
CSF
Volume (cc)
Age (years)
Female Brain/CSF Ratio
c
Ratio
Male Brain/CSF Ratio
d
Age (years)

# Supplemental Figures

Supplemental Figure 1

a

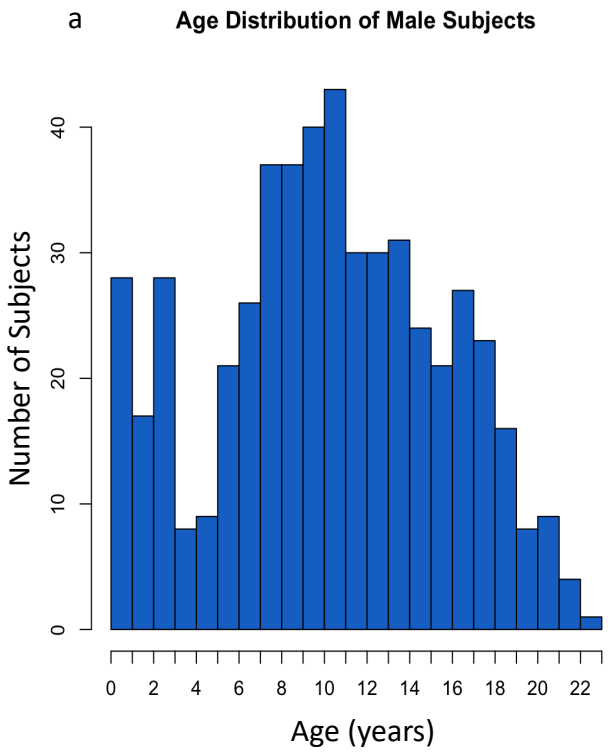


b

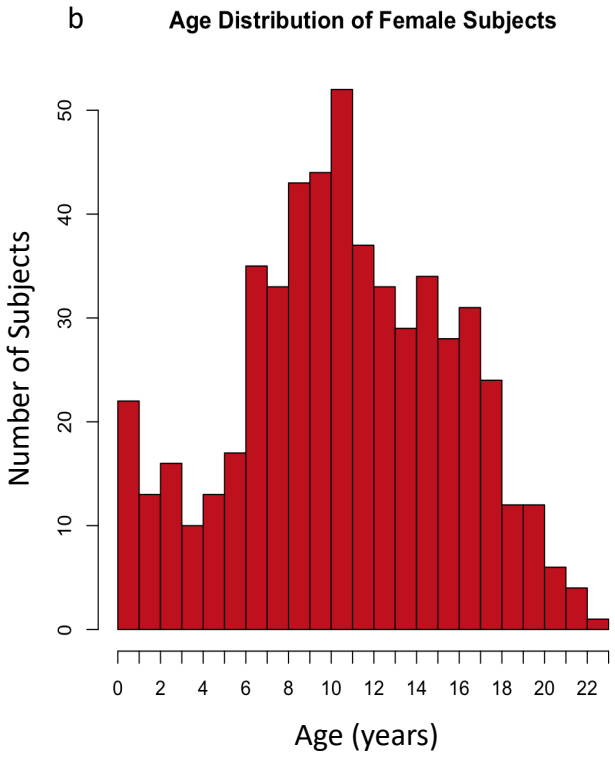


c

| | Female | Male | Total |
|---|---|---|---|
| **Scans** | 549 | 518 | 1067 |
| **Subjects** | 259 | 246 | 505 |
| **Min Age (days)** | 14 | 13 | NA |
| **Max Age (days)** | 8131 | 8073 | NA |

Supplemental Figure 2

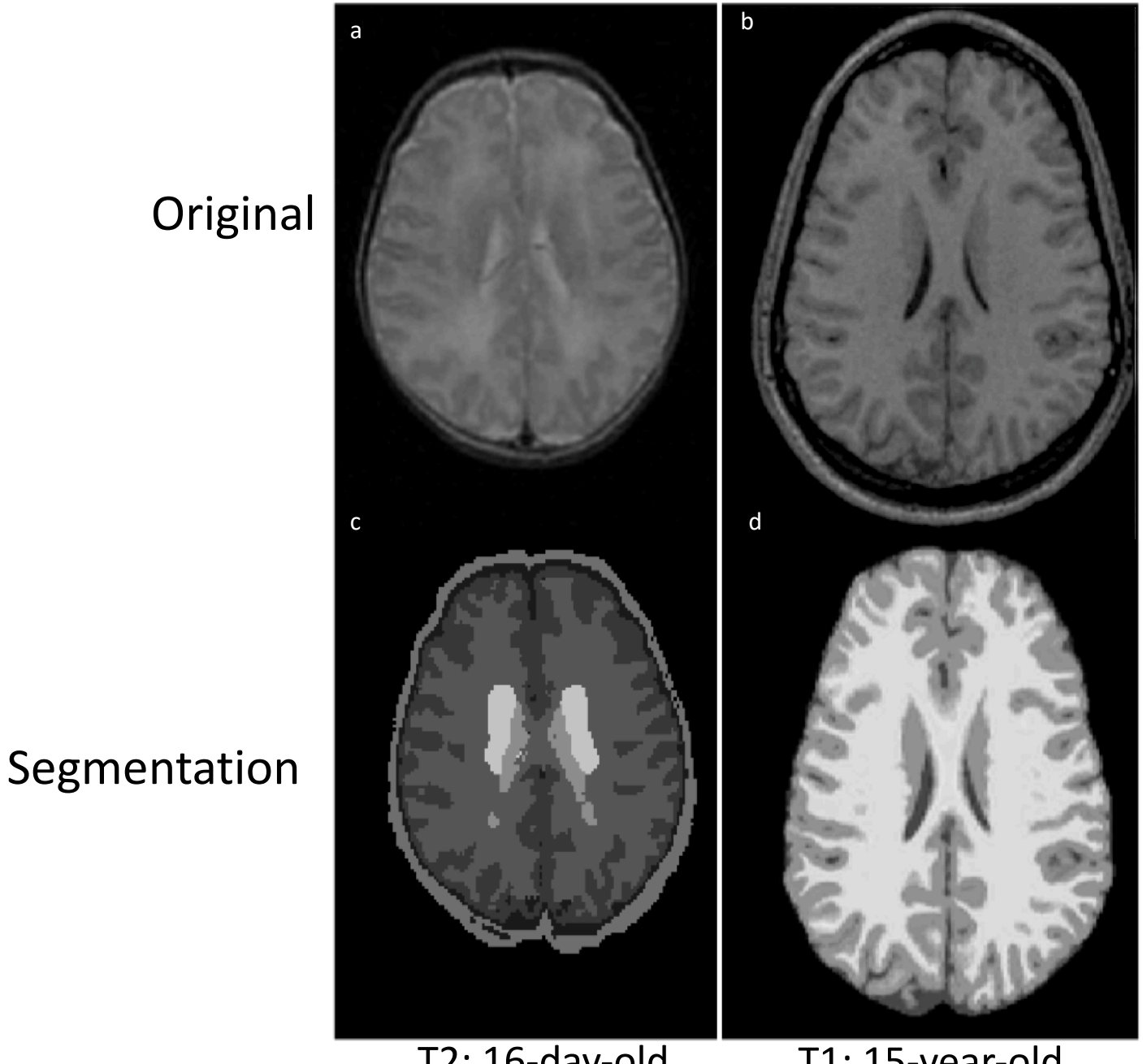

Supplemental Figure 3

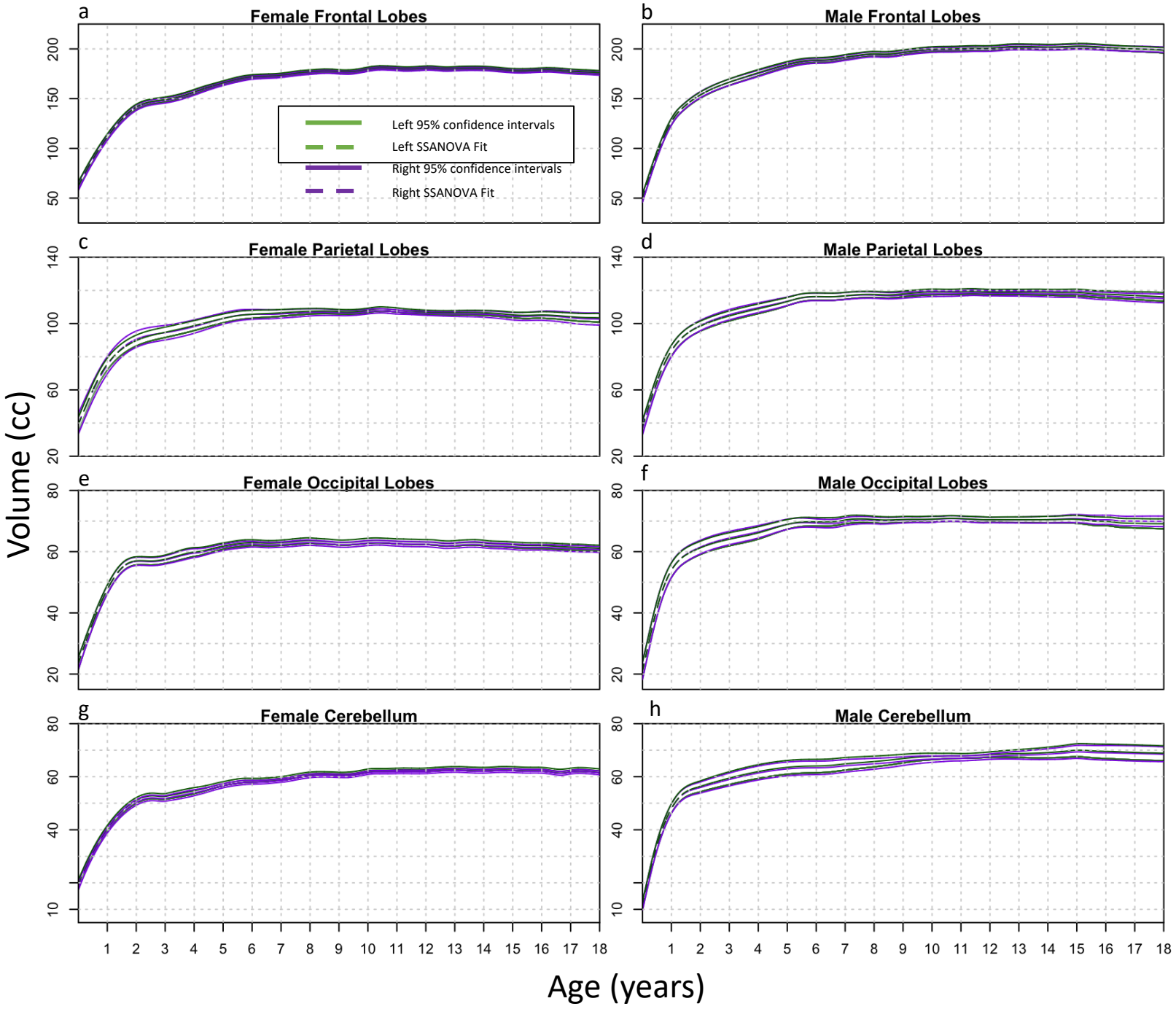

Supplemental Figure 4

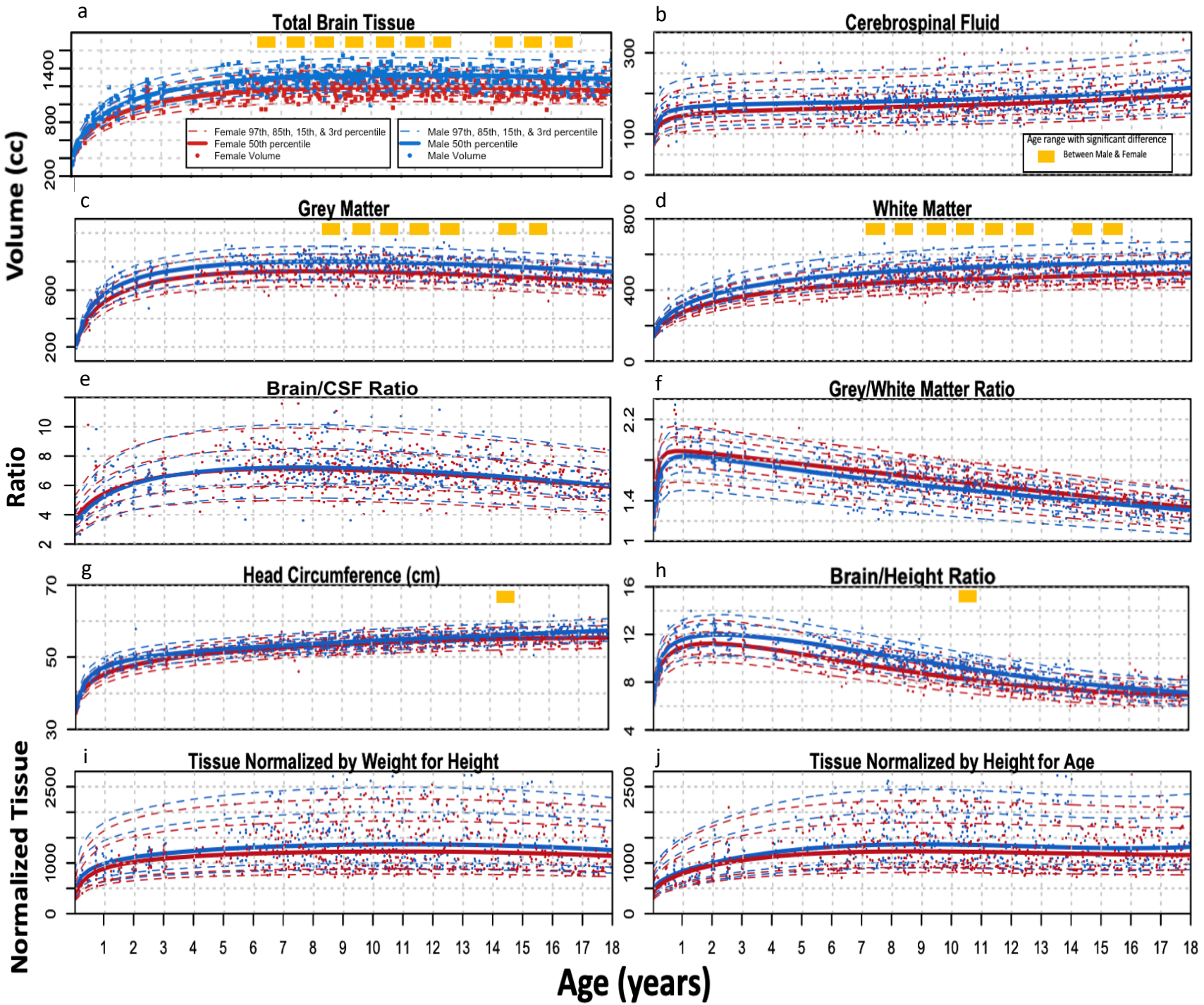

Supplemental Figure 5

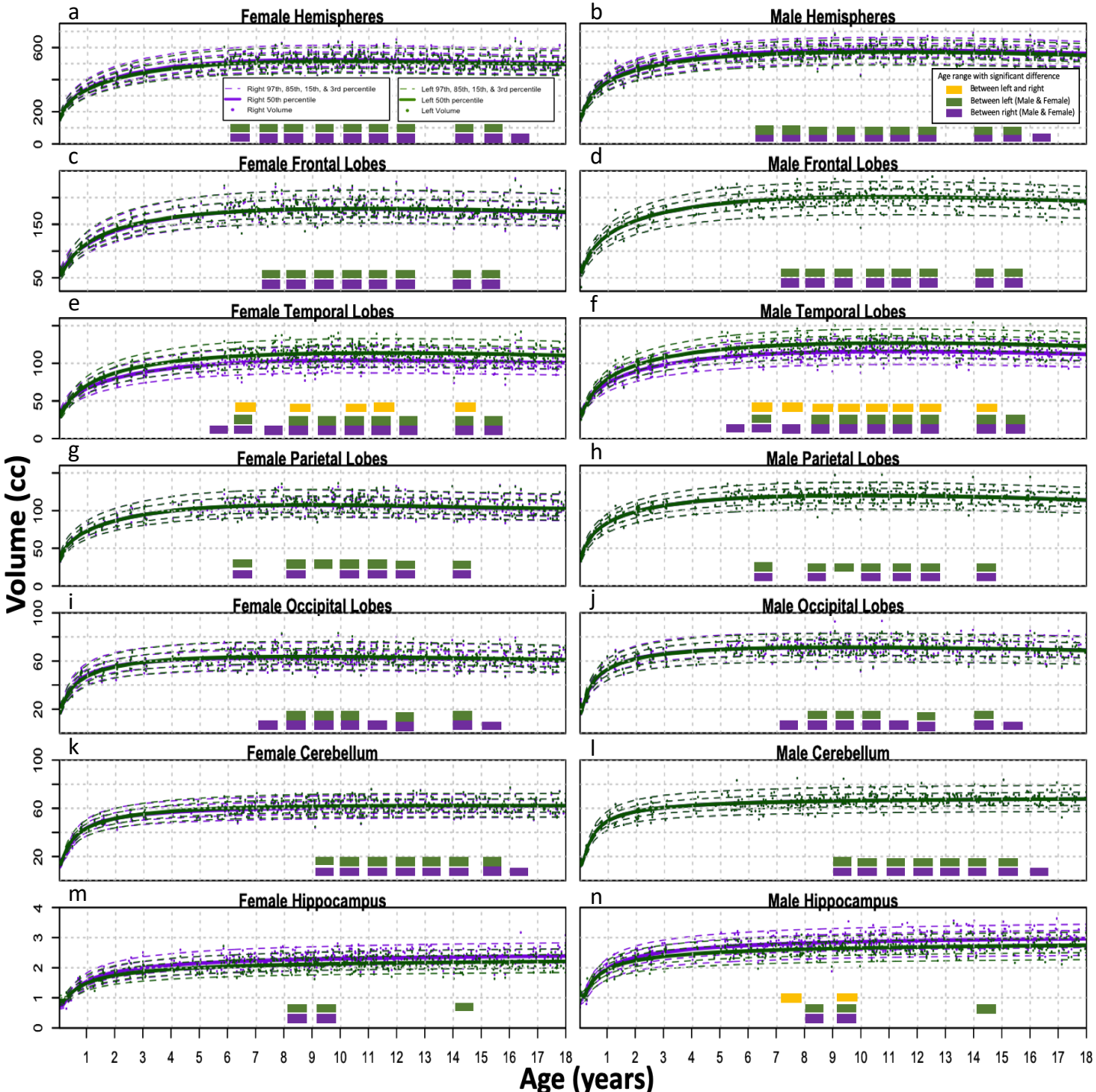
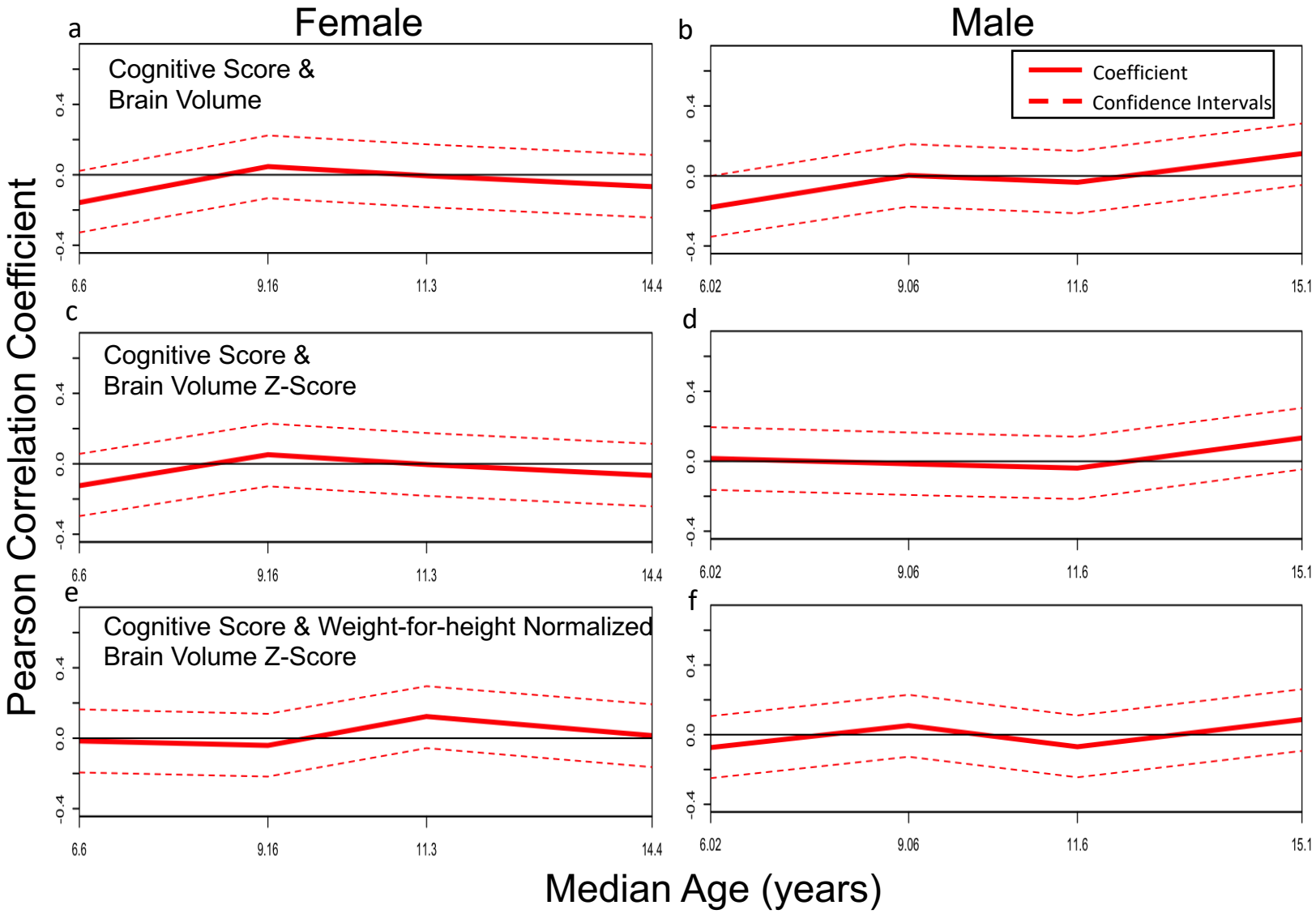
Supplemental Figure 6